Proceedings of the Sixth International Conference on
Railway Technology: Research, Development and Maintenance
Edited by: J. Pombo
Civil-Comp Conferences, Volume 7, Paper 7.5
Civil-Comp Press, Edinburgh, United Kingdom, 2024
ISSN: 2753-3239, doi: 10.4203/ccc.7.7.5

Performance Analysis of FPGA-Based Extended Kalman Filter for Railway Wheelset Parameters Estimation

K. Mal[1,2], B.S. Chowdhry[2], I.H. Kalwar[3], T.D. Memon[4] and T.R. Memon[5]

[1]Sukkur IBA University, Sukkur, Pakistan
[2]NCRA-Condition Monitoring Systems Lab, Mehran University of Engineering & Technology, Jamshoro, Pakistan
[3]Faculty of Engineering Sciences and Technology, Iqra University, Karachi, Pakistan
[4]Center for Artificial Intelligence Research and Optimization, Faculty of Design and Creative Technology, Torrens University, Melbourne, Australia
[5]Department of Electronic Engineering Quaid-e-Awam University of Engineering, Science and Technology, Nawabshah, Pakistan

Abstract

Embedded systems are vital for implementing simulation-based estimators designed to estimate dynamical systems. Field Programmable Gate Arrays (FPGAs) are widely recognized for their hardware flexibility and high processing speed to construct nonlinear condition monitoring systems. The extended Kalman filter (EKF) model is designed in MATLAB and implemented on FPGA in this research study to predict various railway wheelset characteristics under varied track contact conditions. In this context, the National Instruments (NI) myRIO® development board and sbRIO® single-board controller are used to verify the onboard estimation of wheel-rail interaction parameters through Xilinx® System-on-Chip Zynq and Xilinx Spartan-3 FPGA devices, respectively. Both FPGA platforms are used to evaluate the MATLAB simulated dataset for the railway nonlinear wheelset model with different track conditions for the vehicle's accelerating and decelerating operation modes. For functional verification, the EKF-based railway wheelset parameter estimation is synthesized on FPGA devices, and the FPGA findings are consistent with the MATLAB simulation results. The area-performance analysis of both NI embedded boards (myRIO and sbRIO) is presented and these FPGA devices are seen as suitable

for implementation of designed EKF. Functional verification and resource utilization of Xilinx System-On-Chip Zynq and Xilinx Spartan-3 are investigated. It is observed that Xilinx System-On-Chip Zynq FPGA is optimal for the estimation of railway wheelset parameters.

Keywords: condition monitoring, railway wheelset, wheel-rail interaction, FPGA implementation, performance analysis, System-On-Chip, Spartan-3.

1 Introduction

The forces between the wheel and the track determine the rolling stock's dynamic performance [1, 2], and the transmitted tangential force in the wheel-track is known as the adhesion force [3]. Since these forces are rarely measured directly, it is important to estimate the railway vehicle's contact forces using cutting-edge techniques. A model-based technique for estimating the friction coefficient of wheel and rail contact is provided in [4] and uses an unscented Kalman filter. A data-driven method for identifying adhesion between a heavy-haul locomotive's wheel and track is provided in [5] and uses Particle Swarm Optimization (PSO) and Kernel Extreme Learning Machine (KELM). In order to create a slip controller, the traction force is approximated in [6] by using the Kalman filter. In order to provide a more sophisticated braking control system, adhesion characteristics between wheels and rails are assessed in [7] by creating an observer. In order to evaluate the effect on creep forces in wheel-rail interaction, [8] compares theoretical and measured creep curves. Many studies are being conducted to estimate the wheel-track contact conditions; most of these studies make use of model-based methodologies [9, 10].

During the literature review, numerous methods for precise estimation of railway wheel-rail contact conditions are discovered. Research on the implementation of wheelset parameter estimate techniques is lacking, nevertheless. For instance, in [1], the NI myRIO development board is used to build EKF on a Xilinx System-On-Chip Zynq FPGA in order to predict railway wheelset parameters. The state of charge (SOC) estimation of a lithium-ion battery using the FPGA implementation of EKF is demonstrated in [11]. In [12], the position and orientation of an omnidirectional mechatronic system is estimated by developing sensor fusion using EKF on myRIO-1900 via LabVIEW. In [13], a system with LabVIEW is built to build variable-order fractional chaotic systems, which are then implemented on the Xilinx FPGA chip via myRIO-1900. In [14], sigma-delta modulation techniques are used to create an adaptive channel equalizer on MATLAB and FPGA to examine its performance, and implement a better steepest descent algorithm. In [15], the design is mapped on a Xilinx FPGA to analyze the performance of the multiply-accumulate (MAC) unit. A comparative study is conducted on performance analysis of the MAC unit utilizing several non-conventional, non-binary number systems. However, there aren't many published reports in the literature about EKF implementation and performance study on FPGA for wheel-rail contact conditions.

Thus, in order to estimate wheel-rail contact parameters, we expand on the work suggested in [1, 16] in this research paper by developing and implementing the

extended Kalman filter algorithm on two distinct FPGA platforms. The computer-based National Instruments sbRIO single-board controller and myRIO® development board are chosen for this purpose.

This is how the remainder of the paper is structured. Section 2 describes the design and FPGA implementation of EKF, while Section 3 presents the performance analysis of the entire model. The results are examined in detail in part 4, and the conclusion and next steps are covered in section 5.

2 Extended Kalman Filter Design and FPGA Implementation

Wheel-rail contact characteristics have a major impact on railway operation performance, but they are not readily observable. Thus, for a safe and pleasurable train ride, a cutting-edge method for calculating adhesion conditions with real-time implementation is required [3].

2.1 Extended Kalman filter Design

The extension of the railway wheelset parameter estimate, as shown in Refs. [1, 16, 17], is the focus of this research project. Scholars concern the accurate assessment of adhesion conditions and their real-time implementation to be challenging. Since the nonlinear behavior of railway dynamics makes a single Kalman filter inappropriate for the wheel-track interaction system, an extended Kalman filter is employed in a model-based method to predict wheelset parameters. Figure 1 displays the EKF block diagram using the wheelset model.

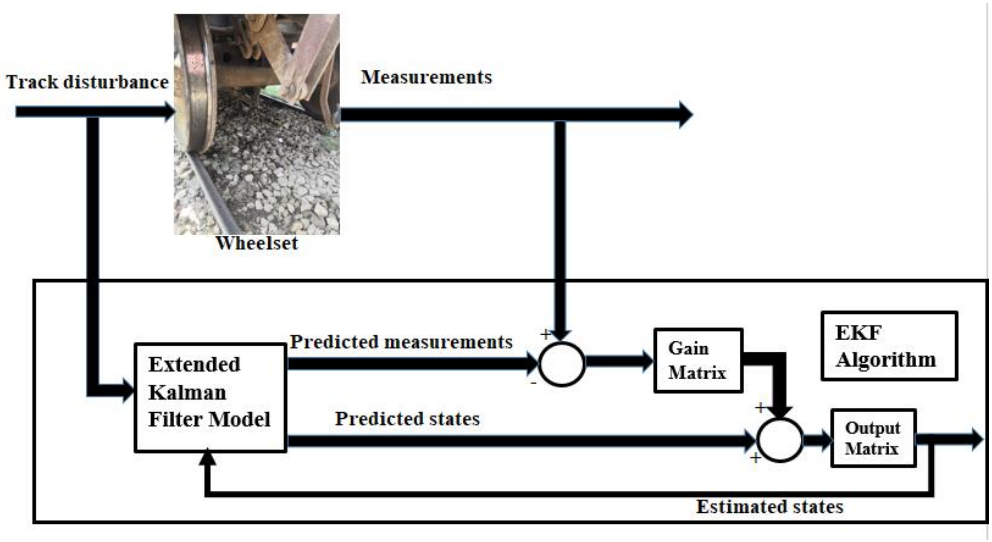

Figure 1: Block diagram of EKF and wheelset model [1]

This nonlinear wheelset model is used in the creation of the EKF algorithm [16]. Equation (1) is provided by developing EKF utilizing the railway wheelset's lateral and yaw motion equations. For state matrix **x**, five variables, such as lateral velocity ($\dot{y}$), yaw rate ($\dot{\Psi}$), slip ratio (γ), friction coefficient (μ), and adhesion force (F_a), are selected and for measurement matrix **m** of the EKF algorithm, lateral acceleration and

yaw rate are selected, as stated in equation (2). Table 1 displays the specific parameters employed in the EKF design for wheelset parameter estimate.

$$\begin{bmatrix} \dot{y} \\ \dot{\Psi} \\ \ddot{y} \\ \ddot{\Psi} \end{bmatrix} = \begin{bmatrix} 0 & 0 & 1 & 0 \\ 0 & 0 & 0 & 1 \\ 0 & \frac{2}{m_w}\frac{F_a}{\gamma} & -\frac{2}{m_w v}\frac{F_a}{\gamma} & 0 \\ -\frac{2L_g\lambda_w}{I_w r_0}\frac{F_a}{\gamma} & -\frac{k_w}{I_w} & 0 & -\frac{2{L_g}^2}{I_w v}\frac{F_a}{\gamma} \end{bmatrix} \begin{bmatrix} y \\ \Psi \\ \dot{y} \\ \dot{\Psi} \end{bmatrix} + \begin{bmatrix} 0 \\ 0 \\ 0 \\ \frac{2L_g}{I_w r_0}\frac{F_a}{\gamma} \end{bmatrix} y_t \quad (1)$$

$$\boldsymbol{x} = [\dot{y} \quad \Psi \quad \gamma \quad \mu \quad F_a]^T, \boldsymbol{m} = [\ddot{y} \quad \dot{\Psi}]^T \quad (2)$$

No.	Notation	Description	Value
1	γ	Slip ratio	-
2	r_0	Radius of wheel	0.5 meter
3	L_g	Track half gauge	0.75 meter
4	λ_w	Wheel conicity	0.15 rad
5	v	Longitudinal velocity of vehicle	m/sec
6	y	Motion in lateral direction	meter
7	y_t	Rail irregularities in lateral direction	meter
8	Ψ	Yaw angle	radians
9	F_a	Adhesion force	Newton
10	I_w	Yaw moment of inertia of wheelset	700 kgm^2
11	k_w	Yaw stiffness	5 x 10^6 N//rad
12	m_w	Wheel weight with induction motor	1250 kg

Table 1: Parameters utilized in EKF design to estimate wheelset parameters.

Using the MATLAB Function tool of Simulink version 9.1, the EKF algorithm shown in Figure 1 is constructed in Simulink for simulation. In Figure 2, the Simulink model is displayed.

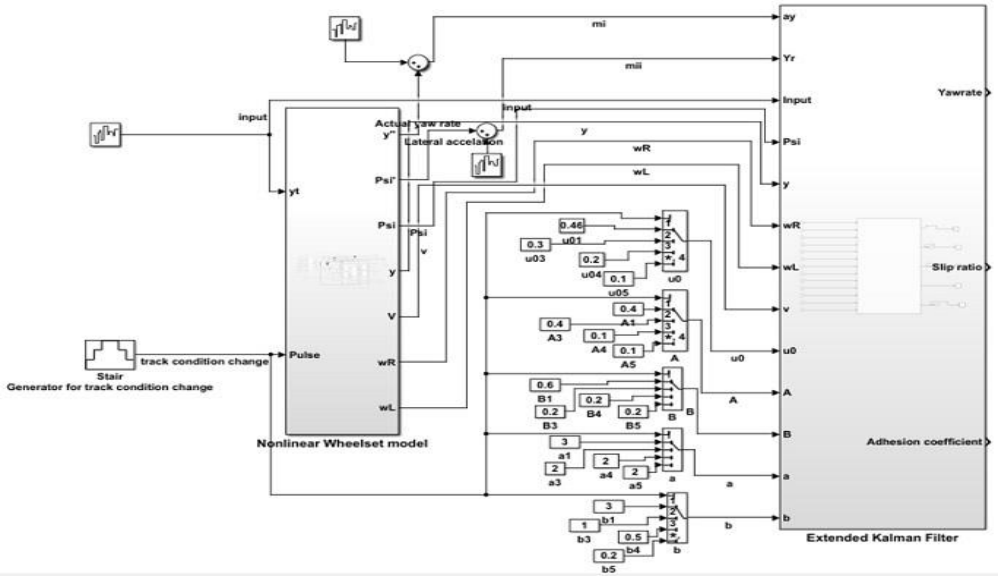

Figure 2: EKF-based simulation model for railway wheelset parameter estimate.

We describe the functional verification, area-performance analysis, and FPGA implementation of the suggested EKF model in the section that follows in order to provide effective predictive maintenance plans.

2.2 FPGA Implementation

Figure 3 displays the block diagram for the entire suggested model. The entire suggested model consists of an FPGA implementation and MATLAB simulation. The simulation component consists of a MATLAB-developed railway wheelset that is explained in [16] and the MATLAB EKF algorithm architecture that is shown in section 2.1. This section provides an explanation of the final portion of the suggested model. Synthesizing any dynamical system across many FPGA platforms is essential for its dependable and effective implementation [18]. The Xilinx System-On-Chip Zynq FPGA integrated into NI myRIO-1900 and the Xilinx Spartan-3 FPGA included into NI sbRIO-9632 are used to implement the EKF that was designed in MATLAB. The purpose of conducting two implementations on distinct architectures is to confirm that the EKF algorithm's structure is independent and to identify a potential FPGA board [19]. An Artix-7 FPGA chip with onboard memory and a dual-core Advanced RISC Machine (ARM) CPU are integrated into computer-based real-time embedded evaluation board known as the NI myRIO®-1900 [20]. The Xilinx Spartan-3 FPGA chip, on the other hand, is incorporated into the NI sbRIO-9632, a CompactRIO Single-Board Controller that offers superior embedment in a variety of applications where high performance and flexibility are required [21]. LabVIEW software, a system-design platform, and a development environment from National Instruments are required for both real-time embedded boards.

The wheelset model simulation dataset, which is stored on solid state drives (SSD) and read by real-time (RT), is streamed to FPGA on each NI embedded board after analysis. The dataset was simulated in MATLAB [16].

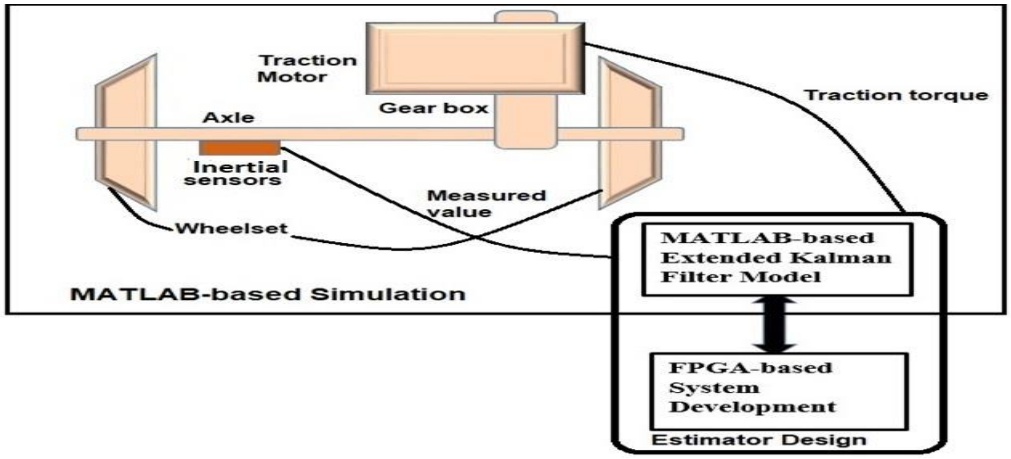

Figure 3: Block diagram of entire suggested model [1].

The NI myRIO and sbRIO boards' operational flow is depicted in the functional block diagram of Figure 4. Each NI embedded board has a solid state drive (SSD) that stores the wheelset model simulation dataset. An ARM CPU reads the SSD, processes it, and streams the data to an FPGA via DMA-FIFO (AXI-4 Stream interface). The internal computation, process Jacobian matrix, measurement Jacobian matrix, and predict-correct algorithm constitute the four primary cores of the FPGA. The

Extended Kalman filter employs a fixed-point data format for both FPGA devices. Using the TCP/IP network interface, the host PC receives results from the FPGA.

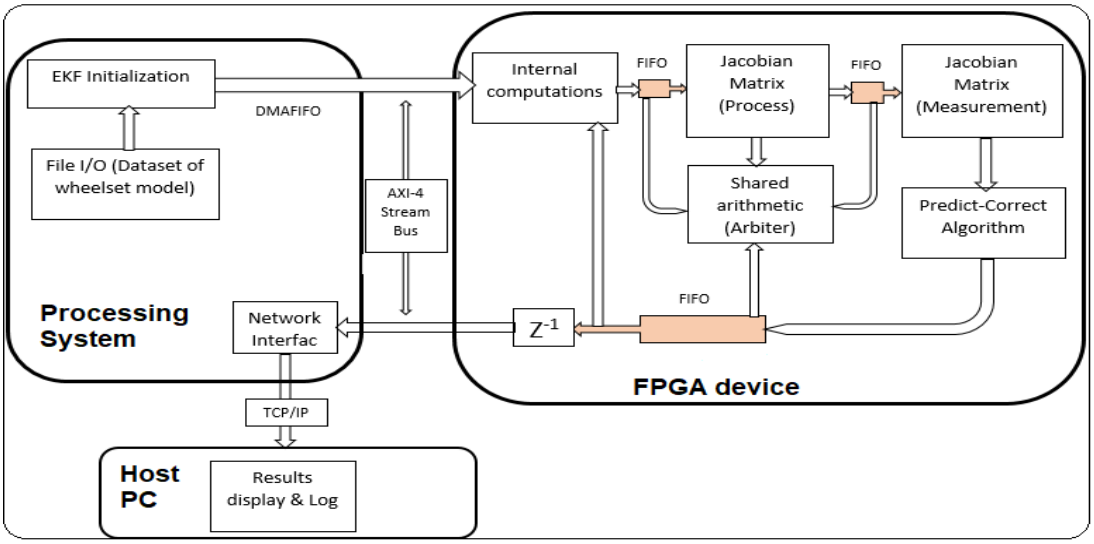

Figure 4: Functional flow diagram of NI myRIO and sbRIO [1].

The chip-area utilizations on Xilinx Zynq and Xilinx Spartan-3 FPGA devices are shown in Table 2 following the synthesis of the suggested model.

Resource Name	FPGA Device	Available	Used	Utilization (%)
CLBs	Xilinx Zynq System-On-Chip	2200	2200	100
	Xilinx Spartan-3	8320	3744	45
Slices	Xilinx Zynq System-On-Chip	4400	4400	100
	Xilinx Spartan-3	16640	7488	45
Block RAMs	Xilinx Zynq System-On-Chip	1620kb	1162kb	71.7
	Xilinx Spartan-3	1728kb	553kb	32
Multipliers/ DSP nodes	Xilinx Zynq System-On-Chip	80	33	41.2
	Xilinx Spartan-3	104	26	25

Table 2: Resource utilization of Xilinx Zynq FPGA and Xilinx Spartan-3 FPGA.

Xilinx Spartan-3 FPGA uses more customizable logic blocks (CLBs) and slices than Xilinx Zynq because the latter ran out of CLBs and slices. Xilinx Zynq, one of the most optimized FPGAs, uses more kbs of Block RAMs and multipliers/DSP nodes

than does the Xilinx Spartan-3 FPGA. Furthermore, each sample produced by the Xilinx Zynq and Xilnx Spartan-3 FPGAs uses 52 clock cycles. This shows an FPGA throughput of 769 kilo samples per second; however, the latency is 20 kilo samples per second. The calculation is displayed in Table 3.

FPGA clock	Time period	No. of clocks per sample	Total time taken per sample	Throughput
40 MHz	25 nano seconds	52	1.3 µseconds (52 cycclesx25 nanosec)	769 KS/second

Table 3: FPGA clock performance calculation.

3 Performance Analysis of Complete Model

Different conditions (e.g., dry, wet, greasy, highly slippery) are investigated to examine the functional behavior of the FPGA-implemented EKF. Figure 5 shows that for wet, greasy, and dry track conditions, the adhesion coefficient with respect to slip ratio varies nonlinearly. The conditions of normal adhesion to low adhesion are shown by these curves. These conditions have been selected to illustrate the EKF algorithm's efficacy in a range of adhesion conditions.

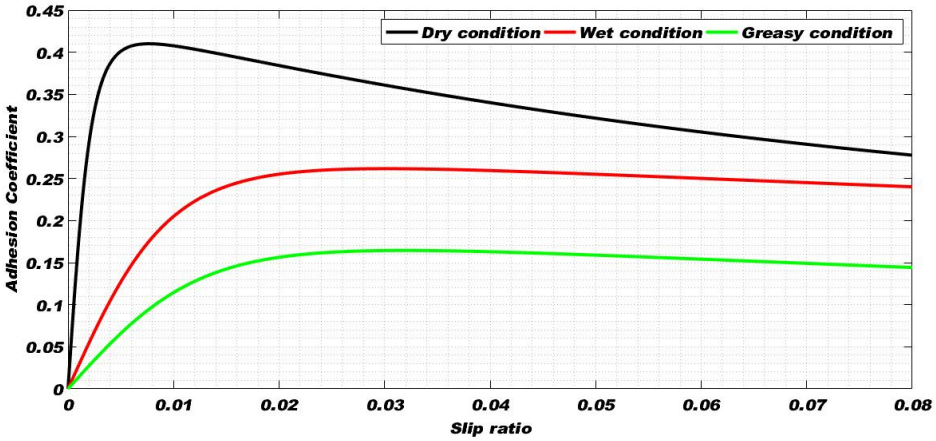

Figure 5: Slip ratio curves for all adhesion conditions.

For a duration of 100 seconds, the complete model comprising a wheelset and an FPGA-based EKF is analyzed (50 seconds during the railway vehicle's accelerating mode and 50 seconds during its decelerating mode). When the track condition is suddenly altered from extremely slippery to dry conditions, the entire model is evaluated. The model receives an input of random track disturbance with an amplitude of ±7 mm to excite lateral dynamics. The initial linear velocity is set at 5 m/sec. The adhesion coefficient, slip ratio, and yaw rate—the three most crucial wheelset parameters—are studied because they affect the dynamics of the complete railway vehicle.

In 50 seconds of operation, the track condition changes from extremely slippery to dry through greasy and wet conditions while operating a railway vehicle. In the

remaining operation, the track condition reverses from dry to extremely slippery. As seen in Figure 6, the vehicle is driven on one track condition for approximately 12.5 minutes, and transition of track from one condition to other is completed in one second.

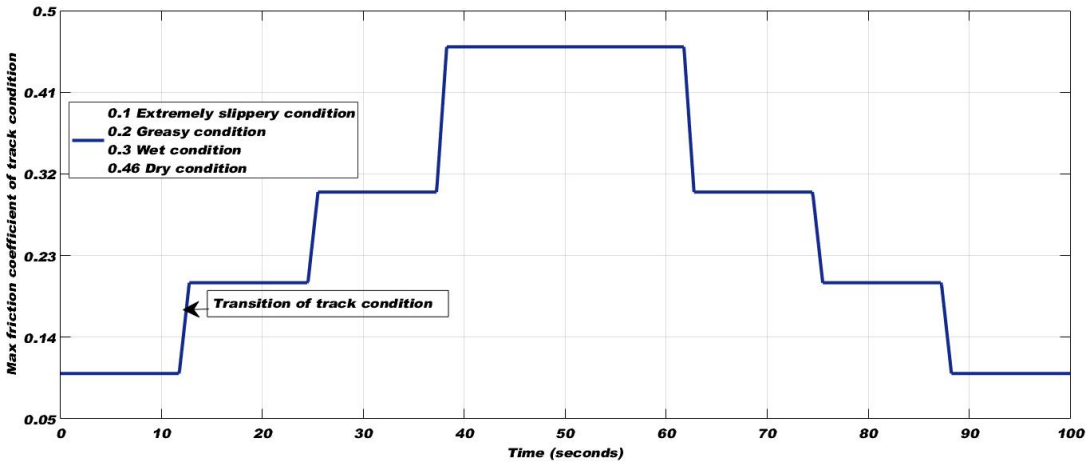

Figure 6: Switching of track conditions duration vehicle operation

During the first 50 seconds of operation, the tractive torque is gradually increased to 5000 Nm in the accelerating mode. This results in a maximum increase in linear velocity of approximately 24 m/sec, or 86.5 km/h. When operating in deceleration mode, torque is applied in the opposite direction to bring the linear velocity down to its initial value. In addition, Figure 7 shows the linear velocity and applied torque.

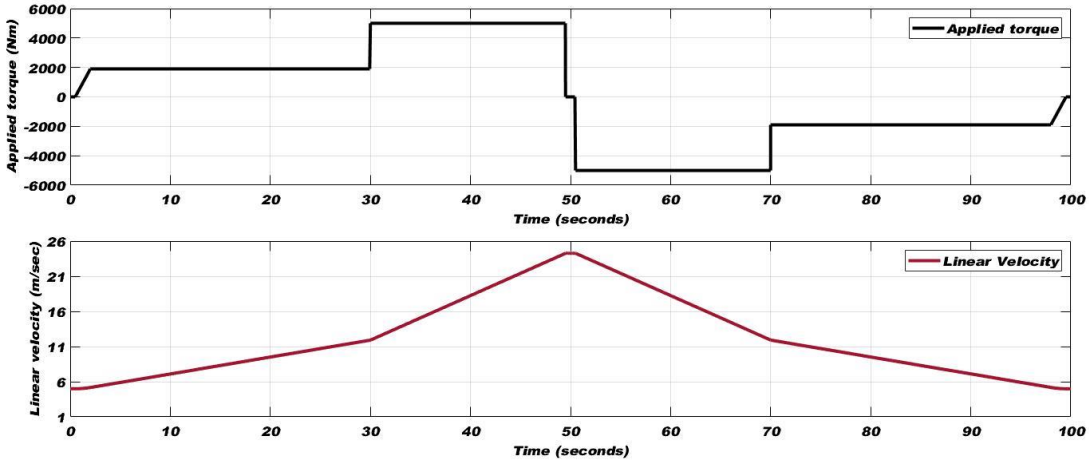

Figure 7: Vehicle forward velocity (bottom) and exerted torque (top) during transition of track conditions

Figure 8 displays the examination of the adhesion coefficient on track condition transition through Simulink, FPGA Zynq, and FPGA Sparta-3. In Simulink, when a track is switched, the estimation error increases significantly; otherwise, the error is minimal. However, because of the complex scenario—which includes lateral track irregularities, traction and brake operation modes, and adhesion condition changes

throughout vehicle operation—a somewhat higher estimating error in adhesion coefficient is generated through both FPGA platforms.

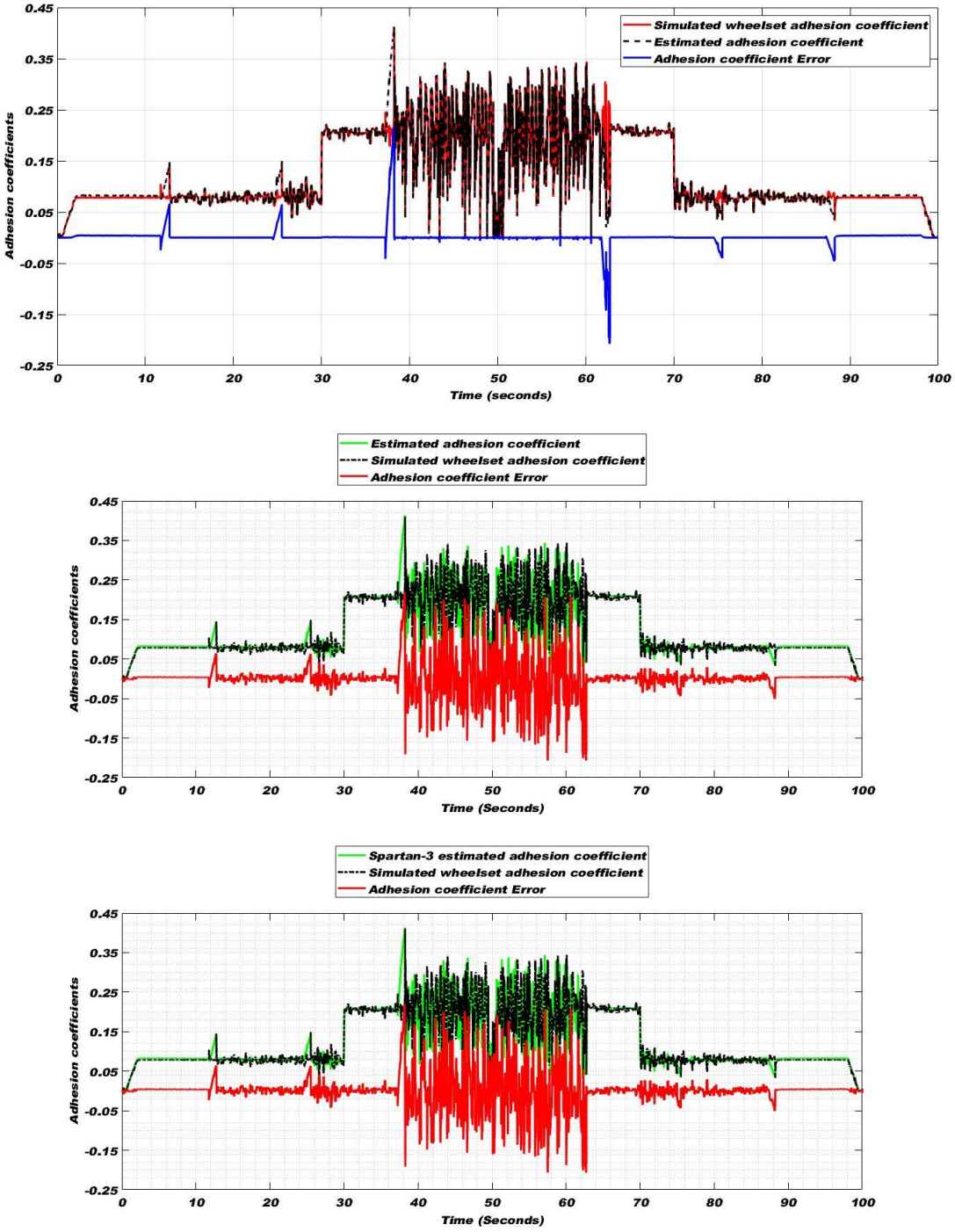

Figure 8: The adhesion coefficient for all conditions on Simulink (top), on FPGA Zynq (middle) and on FPGA Spartan-3 (bottom)

Figure 9 illustrates the assessment of slip ratio during the track condition change using Simulink, FPGA Zynq, and FPGA Sparta-3. The wheelset model's slip ratio is followed with an acceptable inaccuracy by the FPGA-based EKF reaction [22].

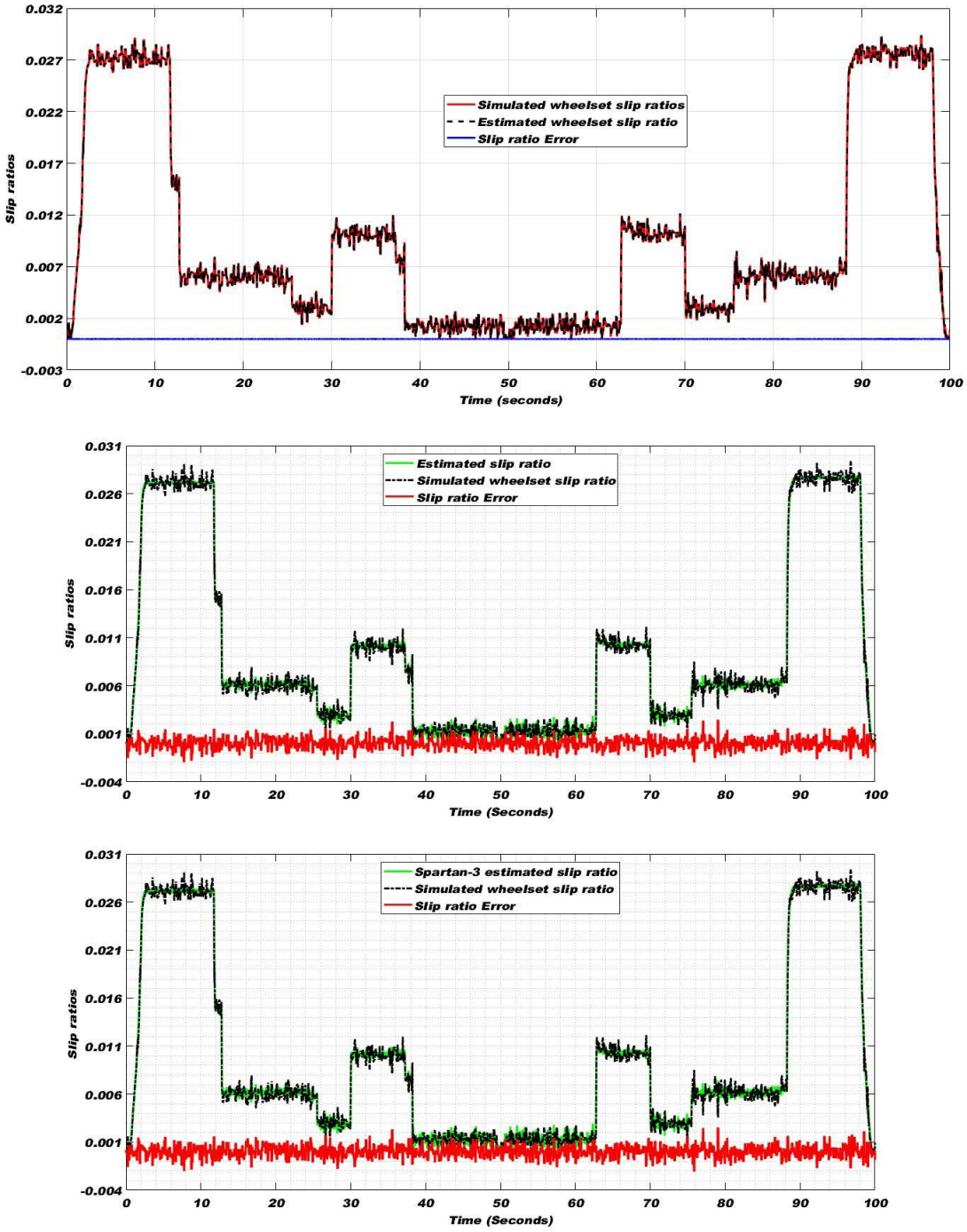

Figure 9: The slip ratio for all conditions on Simulink (top), on FPGA Zynq (middle) and on FPGA Spartan-3 (bottom)

Figure 10 displays the evaluation of the yaw rate on track condition change using Simulink, FPGA Zynq, and FPGA Sparta-3. With relatively minimal estimation error, Zynq FPGA and Spartan-3 respond in a way that matches the wheelset model's yaw rate.

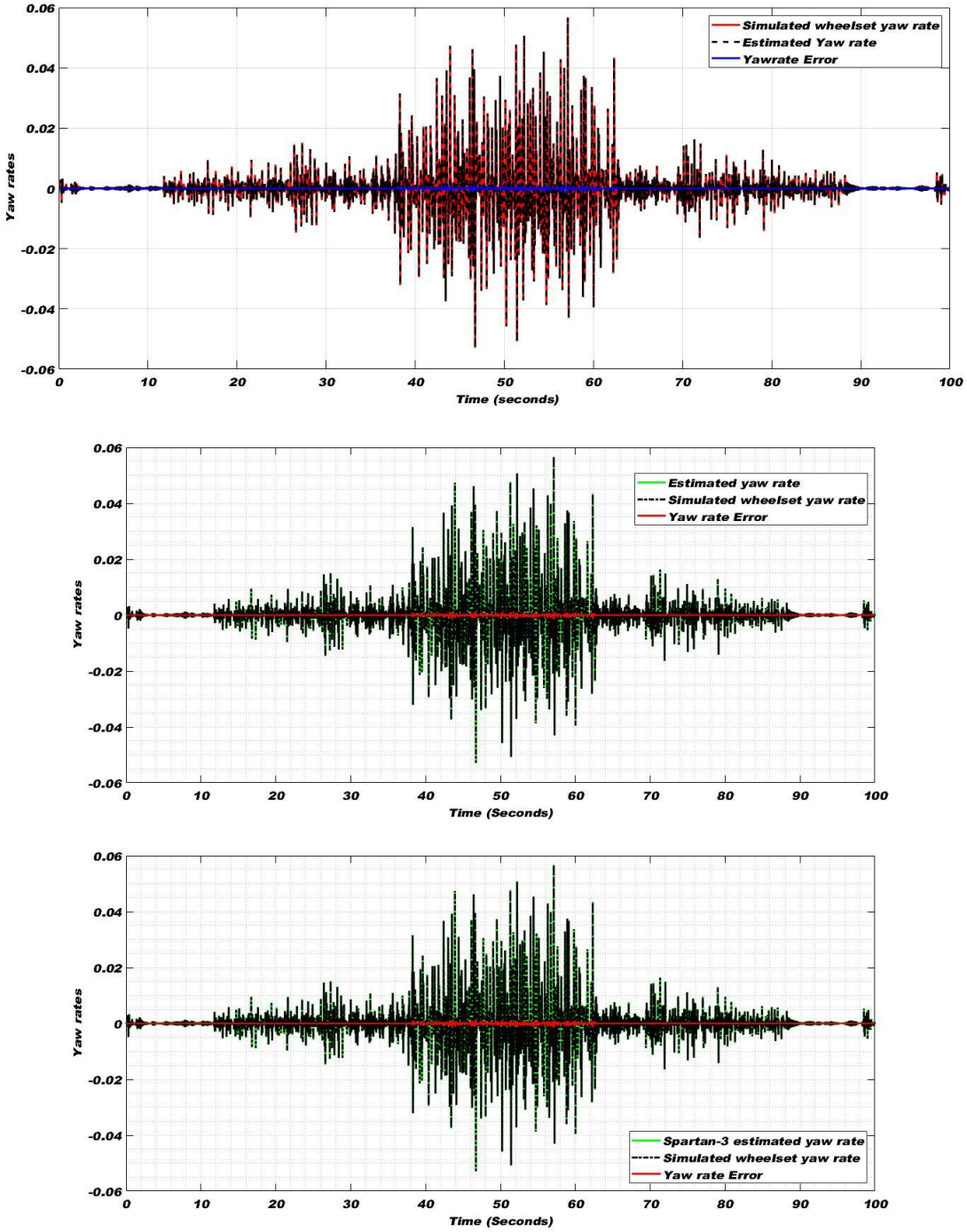

Fig 10: The yaw rate for all conditions on Simulink (top), on FPGA Zynq (middle) and on FPGA Spartan-3 (bottom)

4 Result Discussions

The EKF intended for railway wheelset parameter estimate is implemented on FPGA, as seen in Figures 8 through 10. MyRIO-1900 and sbRIO-9632 are two NI boards that can be used to implement planned EKF for railway wheelset parameter estimate on FPGA.

Equations (3) and (4) are used to compute the relative accuracy index in %, which is used to numerically assess the functional behavior of the EKF-based estimator [22].

$$A = rms(Signal_{est} - Signal_{sim}) \quad (3)$$

$$J = \frac{rms(Signal_{est} - Signal_{sim})}{rms(Signal_{sim})} \quad (4)$$

The first is the absolute accuracy index **A**, which is determined by taking the difference between the simulated and estimated wheelset parameters and calculating its root mean square value (rms). The information from the absolute accuracy index is completed by the second one, the relative accuracy index **J**. Table 4 provides the relative accuracy indices in percentage for forecasting all track conditions.

Track condition	EKF On	Adhesion coefficient			Slip ratio			Yaw rate (rad/sec)		
		A	*rms (Sim)*	J (%age)	A	*rms (Sim)*	J (%age)	A	*rms (Sim)*	J (%age)
Track Transition	Simulink	0.0036	0.072	5.042	3.2257e-6	0.0133	0.024	5.7857e-5	0.0049	1.180
	FPGA Zynq	0.0038		5.274	6.0455e-4		4.535	5.7846e-5		1.178
	FPGA Spartan-3	0.0038		5.275	6.0725e-4		4.555	8.1720e-5		1.664

Table 4: Percentage-based relative accuracy indices

The relative accuracy indices in the percentage are maximum up to 5%, as can be seen in the above table, and this supports the estimator's efficiency. As shown in Figs. 08 and 09, the rms error in percent of adhesion coefficient and slip ratio in both FPGA platforms is considerable. The adhesion coefficient and slip ratio are extremely ephemeral due to lateral track imperfections. The error of yaw rate in greasy and extremely slippery conditions is considerable in Spartan-3 FPGA, as can be observed by zooming into Fig. 10. Complex computation procedures involving tangent inverse functions and square roots are the cause of this inaccuracy. The EKF that was created using Simulink and implemented on two FPGAs has an adequate overall estimation accuracy. Based on the relative accuracy indices provided in Table 4 and the findings of Figures 08 to 10, it can be concluded that the Zynq-7000 FPGA, which is based on myRIO-1900, performs better than the Spartan-3 FPGA, which is incorporated on sbRIO-9632.

4 Conclusions

In this work, the behavior and response of the entire model—which consists of a railway wheelset and an EKF-based estimator—developed in MATLAB are evaluated using Simulink, a Xilinx Spartan-3 FPGA device integrated into an NI sbRIO-9632 single board controller, and a Xilinx System-On-Chip Zynq FPGA chip built into a

computer-based national instrument board myRIO-1900. In order to examine the wheelset parameters estimation accuracy of EKF when the track conditions changed from highly slippery to dry conditions and vice versa during vehicle operation, the analysis was conducted for 100 seconds of railway vehicle operation. On Xilinx Zynq and Xilinx Spartan FPGAs, the Simulink-based EKF is synthesized for functional verification in the accelerating and decelerating operation modes of railway vehicles. Relative accuracy indices are used to quantitatively assess performance, and it is shown that these indices are maximum in percentage terms up to 5%. Overall, it is discovered that the Spartan-3 FPGA integrated on sbRIO-9632 performs worse than the Zynq FPGA based on myRIO-1900. Consequently, the best FPGA implementation of EKF for estimating railway wheelset parameters is Xilinx System-On-Chip Zynq FPGA.

Acknowledgements

The authors would like to acknowledge the "Condition Monitoring Systems Laboratory at Mehran University of Engineering and Technology in Jamshoro, which is a part of the National Center of Robotics and Automation (NCRA) project of the Higher Education Commission of Pakistan", for supporting this work.

References

[1] K. Mal, T. D. Memon, I. H. Kalwar, and B. S. Chowdhry, "FPGA Implementation of Extended Kalman Filter for Parameters Estimation of Railway Wheelset," Comput. Mater. Contin., vol. 74, no. 2, pp. 3351–3370, 2023.

[2] K. Shaikh, I. H. Kalwar, and B. S. Chowdhry, "Wheel Defect Detection Using a Hybrid Deep Learning Approach," Sensors, vol. 6248, pp. 1–15, 2023.

[3] S. Shrestha, Q. Wu, and M. Spiryagin, "Review of adhesion estimation approaches for rail vehicles," Int. J. Rail Transp., vol. 7, no. 2, pp. 79–102, 2019.

[4] Y. Zhao et al, "Real-time wheel–rail friction coefficient estimation and its application," Veh. Syst. Dyn., Published online: 10 Jan 2023.

[5] J. Liu, L. Liu, J. He, C. Zhang, and K. Zhao, "Wheel / Rail Adhesion State Identification of Heavy-Haul Locomotive Based on Particle Swarm Optimization and Kernel Extreme Learning Machine," vol. 2020, no. Journal of Advanced Transportation, 2020.

[6] T. Ishrat, "Slip Control for Trains Using Induction Motor Drive," Queensland University of Technology, 2020.

[7] S. Shrestha, "Estimation of Adhesion Conditions Between Wheels and Rails for the Development of Advanced Braking Control System," Central Queensland University, 2021.

[8] I. Persson, M. Spiryagin, and C. Casanueva, "Influence of non-dry condition creep curves in switch negotiation," Veh. Syst. Dyn., pp. 1–13, 2022.

[9] K. Mal, I. Hussain, T. D. Memon, D. Kumar, and B. S. Chowdhry, "Modern Condition Monitoring Systems for Railway Wheel-Set Dynamics : Performance Analysis and Limitations of Existing Techniques," Sir syed Univ. Res. J. Eng. Technol., vol. 12, no. 1, pp. 31–41, 2022.

[10] M. Zakir et al, “Simulation and analysis of ideal low pass filter response using MATLAB,” Mehran University Research Journal of Engineering and Technology, vol. 42, no. 3, pp. 110–118, 2023.
[11] Y. Ma, P. Duan, P. He, F. Zhang, and H. Chen, “FPGA implementation of extended Kalman filter for SOC estimation of lithium-ion battery in electric vehicle,” Asian J. Control, vol. 21, no. 4, pp. 2126–2136, 2019.
[12] B. Korotaj, B. Novoselnik, and M. Baotic, “Kalman Filter Based Sensor Fusion for Omnidirectional Mechatronic System,” in 2021 International Conference on Electrical Drives & Power Electronics (EDPE), 2021, pp. 183–188.
[13] L. F. Ávalos-Ruiz, C. J. Zúñiga-Aguilar, J. F. Gómez-Aguilar, R. F. Escobar-Jiménez, and H. M. Romero-Ugalde, “FPGA implementation and control of chaotic systems involving the variable-order fractional operator with Mittag–Leffler law,” Chaos, Solitons and Fractals, vol. 115, pp. 177–189, 2018.
[14] T. D. Memon, A. Pathan, and P. Beckett, “FPGA Based Implementation and Area Performance Analysis of Sigma-Delta Modulated Steepest Algorithm for Channel Equalization,” 2018, 12th Int. Conf. Signal Process. Commun. Syst. ICSPCS 2018 - Proc., 2019.
[15] A. Sinha and A. Ghosh, “Comparative performance analysis of FPGA-based MAC unit using non-conventional number system in TVL domain for signal processing algorithm,” Int. J. Nanoparticles, vol. 12, no. 1/2, p. 50, 2020.
[16] K. Mal et al., “A new estimation of nonlinear contact forces of railway vehicle,” Intell. Autom. Soft Comput., vol. 28, no. 3, pp. 823–841, 2021.
[17] K. Mal, I. Hussain, B. Chowdhry, and T. Memon, “Extended Kalman Filter For Estimation Of Contact Forces At Wheel-Rail Interface,” 3C Tecnol., no. Special Issue April 2020, pp. 279–301, 2020.
[18] A. P. D. Nath, S. Ray, A. Basak, and S. Bhunia, “System-on-chip security architecture and CAD framework for hardware patch,” Proc. Asia South Pacific Des. Autom. Conf. ASP-DAC, vol. 2018-Janua, pp. 733–738, 2018.
[19] A. Pathan and T. D. Memon, “Sigma-Delta Modulation Based Single-bit Adaptive DSP Algorithms for Efficient Mobile Communication,” Circuits, Syst. Signal Process., vol. 40, no. 4, pp. 1788–1801, 2021.
[20] N. Instruments, “User Guide and Specifications NI myRIO-1900,” Datasheet, 2016.
[21] A. T. Group, “~ I NI Single-Board RIO Embedded Control.” .
[22] S. Munoz, J. Ros, P. Urda, and J. L. Escalona, “Estimation of Lateral Track Irregularity through Kalman Filtering Techniques,” IEEE Access, vol. 9, pp. 60010–60025, 2021.